Chemical Science

ROYAL SOCIETY OF CHEMISTRY

EDGE ARTICLE

View Article Online
View Journal | View Issue

Cite this: *Chem. Sci.*, 2026, **17**, 7310

All publication charges for this article have been paid for by the Royal Society of Chemistry

Received 30th October 2025
Accepted 8th February 2026

DOI: 10.1039/d5sc08399k

rsc.li/chemical-science

Dinitrogen complexes N_2L_2 (L = N_2, CO, CS, NO^+, CN^-)

Yahui Li,[a] Chengxiang Ding,[a] Lianbin Xie,[a] Sudip Pan *[a] and Gernot Frenking *[bcd]

Quantum chemical calculations using *ab initio* methods and density functional theory have been carried out on the equilibrium structures and the vibrational spectra of the (valence) isoelectronic compounds N_2L_2 (L = N_2, CO, CS, NO^+, CN^-). The molecules have a *trans*-periplanar arrangement of the L_2 ligands at the N_2 unit. The complexes with L = N_2, CO, NO^+, CN^- are predicted as thermodynamically unstable for dissociation into N_2 + 2L with ΔG^{298} value lying in between −257 kcal mol^{-1} (L = NO^+) and −73 kcal mol^{-1} (L = CO), but the adduct $N_2(CS)_2$ is calculated as slightly stable with ΔG^{298} = 4 kcal mol^{-1}. The homolytic dissociation reaction into two fragments N_2L_2 → 2 NL is energetically less favorable than the heterolytic fragmentation N_2L_2 → N_2 + 2 L, which proceeds synchronously but asymmetrically. The activation barriers for the fragmentation reaction N_2L_2 → N_2 + 2L have values between $\Delta G^{\neq}$(298 K) = 17 kcal mol^{-1} for L = N_2 and $\Delta G^{\neq}$(298 K) = 84 kcal mol^{-1} for L = CS. The calculated vibrational frequencies suggest that the molecules N_2L_2 can be identified by the IR active antisymmetric stretching mode ν_{as} of the ligands L, which is blue shifted for L = CO (Δ = 55 cm^{-1}) and L = NO^+ (Δ = 118 cm^{-1}) but it is red shifted for L = CS (Δ = −242 cm^{-1}) and L = CN^- (Δ = −133 cm^{-1}) relative to the ν_{as} mode of L = N_2. The analysis of the bonding situation reveals that there is a total charge donation L→($^1\Gamma$-N_2)←L in all complexes, ranging between 1.38 *e* (L = CN^-) and 0.56 *e* (L = N_2), except in the dication with L = NO^+, where a small backdonation in reverse direction L←($^1\Gamma$-N_2)→L with 0.10 *e* is calculated. EDA-NOCV calculations of N_6 show that the best description of the bonding situation is given in terms of dative interactions N_2→($^1\Gamma$-N_2)←N_2 between central N_2 in the excited $(1)^1\Gamma_g$ singlet state and the terminal N_2 fragments in the $^1\Sigma_g^+$ electronic ground state. In contrast, the best description of the complexes with L = CO, CS, NO^+ is calculated for the interactions between the central N_2 in the $^5\Sigma_u^+$ quintet state and the terminal ligands in the symmetry-adapted $(L)_2$ quintet state. For N_2L_2 with L = CN^-, it is found that the bonding is best described for the interaction between N_2^- in the electronic quartet ($^4\Sigma_u^+$) state and the terminal $(L)_2^-$ ligand as symmetry-adapted quartet. In contrast to the common bonding model for N_6 using Lewis structures $N^-{=}N^+{=}N{-}N{=}N^+{=}N^-$, the donor–acceptor model N_2→(N_2)←N_2 explains that the lowest activation barrier is found for the concerted cleavage of the two formal double bonds, leading to the experimentally observed dissociation into 3 N_2.

Introduction

In 1964, Appel and Schöllhorn reported that triphenylphosphinazine, which was sketched with the formula $Ph_3P{=}N{-}N{=}PPh_3$, is a thermally stable diamagnetic species that has a melting point of 184°.[1] However, neither precise structural information about the compound was given in the work, nor in their further study.[2] Later, quantum chemical calculations showed that $N_2(PPh_3)_2$ is thermodynamically unstable for the release of N_2 by ∼90 kcal mol^{-1},[3] which raised doubts about the structure of the isolated compound. A subsequent X-ray structure analysis confirmed that the species is indeed triphenylphosphinazine, which has an antiperiplanar arrangement of the phosphine groups in Ph_3P-(N_2)-PPh_3 with bending angles P–N–N of 107°, and a long N–N bond of 1.497 Å.[4] The theoretical analysis of the bonding situation suggested that the N_2 moiety binds through its highly excited $(1)^1\Gamma_g$ state, where the out-of-plane π and π* orbitals are doubly occupied and the in-plane π MO is vacant, which leads to strong dative interactions Ph_3P→(N_2)←PPh_3 with N_2 as a double Lewis acid. The same type of dative interactions was suggested for the related compound with NHC (N-Heterocyclic Carbene) ligand, NHC→(N_2)←NHC, which was reported to have an

[a]*Institute of Atomic and Molecular Physics, Jilin University, Changchun 130023, China. E-mail: sudip@jlu.edu.cn*

[b]*Institute of Advanced Synthesis, School of Chemistry and Molecular Engineering, Nanjing Tech University, Nanjing 211816, China. E-mail: frenking@chemie.uni-marburg.de*

[c]*Fachbereich Chemie, Philipps-Universität Marburg, Hans-Meerwein-Strasse 4, D-35043 Marburg, Germany*

[d]*Donostia International Physics Center (DIPC), M. de Lardizabal Pasealekua 3, 20018 Donostia, Euskadi, Spain*

antiperiplanar arrangement of the NHC groups and a long N–N bond of 1.415 Å.[5]

Very recently, Qian, Mardyukov and Schreiner (QMS) reported the synthesis, *via* gas-phase reaction, of the new nitrogen allotrope N_6, which was trapped in low-temperature argon matrices at 10 K and as a film at liquid nitrogen temperature of 77 K.[6] The molecule was identified by IR and UV-vis spectroscopy, and by *ab initio* calculations, which predict a structure where two N_3 fragments are bonded in a *trans*-arrangement through a long (1.460 Å) N–N bond. The viewpoint of N_6 as the dimer of N_3 is reasonable, because hexanitrogen was synthesized by treating AgN_3 with Cl_2, which yields ClN_3 that reacts with AgN_3 and leads to the formation of the new nitrogen allotrope N_6. Hexanitrogen was heralded as a molecule of the year 2025 wth a long N–N bond connecting two N_3 fragments.[7] But the structural similarity to the $N_2(PPh_3)_2$ and $N_2(NHC)_2$ species led us suspect that the N_6 species is another example of the compound class N_2L_2 where the ligands L are bonded through dative interactions $L\rightarrow(^1\Gamma\text{-}N_2)\leftarrow L$. Dinitrogen N_2 is generally known as weakly bonded ligand, but the highly excited $(1)^1\Gamma_g$ state of the central N_2 is a strong σ acceptor and strong π donor, which is capable to bind two N_2 ligands. The $(1)^1\Gamma_g$ state of N_2 is 294.3 kcal mol^{-1} above the $X^1\Sigma_g^+$ ground state,[8] which, however, does not occur in N_2L_2 as a free species, but as a reference state that is strongly stabilised by orbital interactions.

Another acceptor, which binds even eight N_2 ligands in the octa-coordinated complexes $M(N_2)_8$ (M = Ca, Sr, Ba), is the alkaline-earth atom M in an excited triplet state with $(n-1)d^2$ electron configuration *via* strong $M\rightarrow(N_2)_8$ π backdonation.[9]

The new findings prompted us to investigate the electronic structure of N_6 in terms of dative bonding $N_2\rightarrow(^1\Gamma\text{-}N_2)\leftarrow N_2$ and to compare the homolytic and heterolytic bond dissociation with quantum chemical methods. We also calculated the (valence) isoelectronic compounds N_2L_2 (L = N_2, CO, CS, NO^+, CN^-). Here, we report about the equilibrium geometries, bond dissociation energies (BDEs), and the vibrational spectra of the molecules. We also present a thorough analysis of the nature of the chemical bonds using a variety of methods. The results may be useful as a guideline for future experimental studies.

Methods

The geometrical optimizations, followed by the frequency calculations of N_2L_2 (L = N_2, CO, CS, NO^+, CN^-) compounds, were first carried out at the M06-2X/cc-pVTZ level[10] in their respective singlet and triplet spin states. Taking the most stable spin state (singlet), further reoptimizations and frequency calculations were performed at the CCSD(T)-Full/cc-pVTZ level.[11] These calculations were done using the Gaussian 16 program.[12] Natural atomic charges and Mayer bond order[13] were calculated using NBO7 (ref. 14) and Multiwfn programs,[15] respectively.

Energy decomposition analysis (EDA)[16] in conjunction with the natural orbital for chemical valence theory (NOCV)[17] was carried out at the M06-2X/TZ2P-ZORA[18]//CCSD(T)/cc-pVTZ level using the ADF 2020 package.[19] The ZORA method considers relativistic effects, which are unimportant for this work, but further work by us on heavier analogues requires a uniform level of theory. In the EDA-NOCV[20] analysis, the intrinsic interaction energy (ΔE_{int}) between two fragments is dissected into three distinct energy components, as follows:

$$\Delta E_{int} = \Delta E_{elstat} + \Delta E_{Pauli} + \Delta E_{orb} \quad (1)$$

The electrostatic ΔE_{elstat} term represents the quasiclassical electrostatic interaction between the unperturbed charge distributions of the prepared fragments. The Pauli repulsion, ΔE_{Pauli} accounts for the energy change during the transformation from the superposition of unperturbed electron densities of the individual fragments to a wavefunction that explicitly adheres to the Pauli principle, achieved through the necessary antisymmetrization and wavefunction renormalization. The orbital term ΔE_{orb} comes from the mixing of orbitals, charge transfer, and polarization between the isolated fragments.

The EDA-NOCV enables the partition of the total ΔE_{orb} into pairwise contributions of the orbital interactions that are very important to get a complete picture of the bonding. The charge deformation $\Delta\rho_k(r)$, resulting from the mixing of the orbital pairs $\psi_k(r)$ and $\psi_{-k}(r)$ of the interacting fragments presents the amount and the shape of the charge flow due to the orbital interactions (eqn (2)), and the associated energy term ΔE_{orb} provides with the size of stabilizing orbital energy originated from such interaction (eqn (3)).

$$\Delta\rho_{orb}(r) = \sum_k \Delta\rho_k(r) = \sum_{k=1}^{N/2} \nu_k\left[-\psi_{-k}^2(r) + \psi_k^2(r)\right] \quad (2)$$

$$\Delta E_{orb} = \sum_k \Delta E_{orb}{}^k = \sum_k \nu_k\left[-F_{-k,-k}^{TS} + F_{k,k}^{TS}\right] \quad (3)$$

Several papers extensively discussed details of the EDA-NOCV method and its application, offering different perspectives and viewpoints.[21]

Results and discussion

Fig. 1 shows the calculated geometries, atomic partial charges (q), and bond orders (P) of the compounds N_2L_2 (L = N_2, CO, CS, NO^+, CN^-) at the CCSD(T)/cc-pVTZ level. All molecules exhibit a *trans*-periplanar arrangement of the L_2 ligands at the N_2 unit with a C_{2h} point group and ^1A_g electronic state. The singlet-triplet gap computed at the M06-2X/cc-pVTZ level is very high (39.7–65.7 kcal mol; see Table S1 in SI). The central N–N bond lengths in $N_2(N_2)_2$ (1.450 Å) and $[N_2(CN)_2]^{2-}$ (1.488 Å) compare favorably with the bond length in $H_2N\text{–}NH_2$ (1.445 Å),[6] whereas the N–N bonds in $N_2(CO)_2$ (1.386 Å), $N_2(CS)_2$ (1.355 Å) and $[N_2(NO)_2]^{2+}$ (1.382 Å) are significantly shorter. The small differences between our values for N_6 and the data reported by QMS are due to the fact that the CCSD(T)/cc-pVTZ calculations were carried out by us with the full core option, whereas the previous study used the frozen core approximation. Geometry optimisations of a *syn* isomer did not result in another

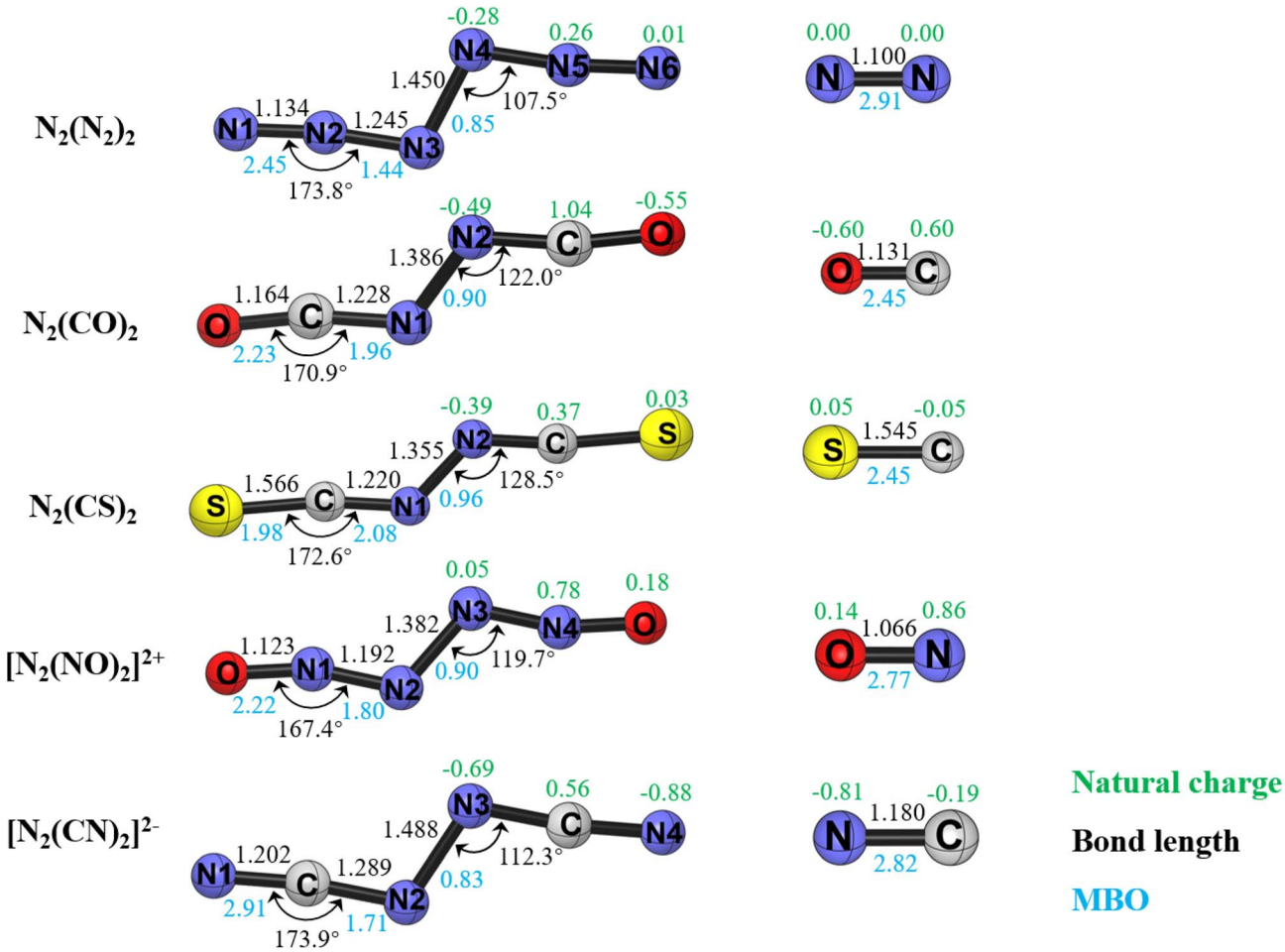

Fig. 1 Minimum energy geometries, partial charges (q) and bond orders (P) of the N_2L_2 (L = N_2, CO, CS, CN^-, NO^+) compounds and the ligands L at the CCSD(T)/cc-pVTZ level. The bond lengths are given in Å, bond angles in degree. All molecules have a C_{2h} point group and ^1A_g electronic state.

conformational isomer, but rather in the *trans* form as the only acyclic energy minimum structure. An extensive search of the potential energy surface using various starting geometries gave planar four-membered cyclic structures $N_2(CX)_2$ (X = O, S) as energy minima, which are > 25 kcal mol^{-1} less stable than the acyclic N_2L_2 forms. We also located nonplanar four-membered cyclic isomers for all species except for N_6 where the central N–N bond is broken, which are > 40 kcal mol^{-1} higher in energy than the acyclic N_2L_2 forms. They are shown in Fig. S1 of the SI. Since the present work focuses on the dinitrogen complexes N_2L_2, we do not discuss the cyclic isomers in this work.

Table 1 gives the calculated BDEs for the fragmentation N_2L_2 → N_2 + 2L at the CCSD(T)/cc-pVTZ level, which show a remarkably high variation. The purely electronic values suggest that $[N_2(NO)_2]^{2+}$ is even less stable (D_e = −233.3 kcal mol^{-1}) than $N_2(N)_2$ (D_e = −179.1 kcal mol^{-1}). The exoenergetic values are much lower for $[N_2(CN)_2]^{2-}$ (D_e = −116.7 kcal mol^{-1}) and $N_2(CO)_2$ (D_e = −49.5 kcal mol^{-1}), and $N_2(CS)_2$ is even predicted to be energetically stable (D_e = 27.7 kcal mol^{-1}). The corrections by vibrational frequencies and entropic and thermal contributions lead to ΔG^{298} values where the N_2L_2 compounds are seen as thermodynamically unstable in the order L = NO^+ > N_2 > CN^- > CO, but the molecule $N_2(CS)_2$ is calculated as thermodynamically stable at room temperature with ΔG^{298} = 3.6 kcal mol^{-1}.

Table 1 Computed bond dissociation energies D_e, zero-point energies corrected bond dissociation energies D_0, enthalpy change ΔH and free energy change ΔG of the processes (a) N_2L_2 → N_2 + 2L and (b) N_2L_2 → 2NL at the CCSD(T)/cc-pVTZ level. All values are given in kcal mol^{-1}

Complex	D_e	D_0	ΔH	ΔG
(a) N_2L_2 → N_2 + 2L				
$N_2(N_2)_2$	−179.1	−184.1	−182.0	−200.7
$N_2(CO)_2$	−49.5	−55.8	−53.7	−73.4
$N_2(CS)_2$	27.7	21.8	23.6	3.6
$[N_2(CN)_2]^{2-}$	−116.7	−122.2	−120.1	−139.7
$[N_2(NO)_2]^{2+}$	−233.3	−238.7	−236.5	−256.8
(b) N_2L_2 → 2NL				
$N_2(N_2)_2$	34.4	29.6	30.5	22.2
$N_2(CO)_2$	62.1	58.5	59.1	48.9
$N_2(CS)_2$	27.8	24.1	25.0	13.4
$[N_2(CN)_2]^{2-}$	−51.8	−56.8	−55.8	−60.8
$[N_2(NO)_2]^{2+}$	−70.2	−74.5	−73.7	−84.6

Table 1 also gives the BDEs for breaking the central N–N bond in the fragmentation $N_2L_2 \rightarrow 2$ NL at the CCSD(T)/cc-pVTZ level. It becomes obvious that the homolytic bond rupture of the N–N bond is thermodynamically strongly disfavoured compared with the heterolytic cleavage of the L–N_2–L bonds, except for L = CS. The energies of the two fragmentation reactions of the latter species are very similar, but the free energy of the heterolytic process ($\Delta G = 3.6$ kcal mol^{-1}) makes it clearly more favourable than the homolytic fragmentation ($\Delta G = 13.4$ kcal mol^{-1}). The calculated BDEs at the M06-2X/cc-pVTZ level are very similar (Table S2 of SI) to the CCSD(T)/cc-pVTZ values, which indicates that the DFT values are quite reliable.

Fig. 2 shows the reaction profile for the heterolytic dissociation reaction $N_2L_2 \rightarrow N_2 + 2$ L along with the calculated activation free energy barriers $\Delta G^{\neq}$(298 K), which vary between 16.9 kcal mol^{-1} (L = N_2) and 84.2 kcal mol^{-1} (L = CS). The trend of the $\Delta G^{\neq}$ follows, in general, the reaction energies, except for the very exergonic reactions where L = N_2, NO^+. The calculated barrier for the fragmentation of N_2 is in good agreement with the value reported by QMS (14.8 kcal mol^{-1}).[6] The computed value of the T_1 diagnostics suggests that the multi-reference character of the CCSD(T) calculations of the N_2L_2 complexes and the transition states is very low (Table S3, SI), which indicates that the single-reference approach is sufficient. The activation barrier for the homolytic reaction $N_6 \rightarrow 2\ N_3$ was reported by QMS to be significantly higher ($\Delta G^{\neq}$(298 K) = 26.1 kcal mol^{-1}) than the heterolytic process.[6] We carried out energy calculations with stretched N–N distances of the other L_2L_2 species, which suggest that the barriers are also higher than for the heterolytic fragmentation. Since the NL fragments are also less stable than N_2 + 2 L (Table 1), it is unlikely that the homolytic reaction course plays a role in the fragmentation reaction of the N_2L_2 species.

The higher barrier for breaking the bond in the central N_2 moiety of N_6 compared to breaking the (N_2)–$(N_2)_2$ bonds is surprising, given the calculated bond orders, which are much higher and have shorter distances in the latter bonds than the former one. It turns out that the energy required to break a bond depends not only on the strength of the bond, but also on the reorganisation of the electronic structure of the fragments during the cleavage reaction. The N_3–N_3 bond in N_6 is weaker than the (N_2)–$(N_2)_2$ bonds, but the electronic charge migration during rupture of the latter heterolytic process is energetically more favourable than the homolytic reaction. The lower barrier for breaking the (N_2)–$(N_2)_2$ bonds than the N_3–N_3 bond supports the use of our bonding model for N_6 in terms of dative interactions $N_2 \rightarrow (N_2) \leftarrow N_2$ rather than the more conventional model using Lewis structures $N^- \!=\! N^+ \!=\! N\text{–}N \!=\! N^+ \!=\! N^-$, since it

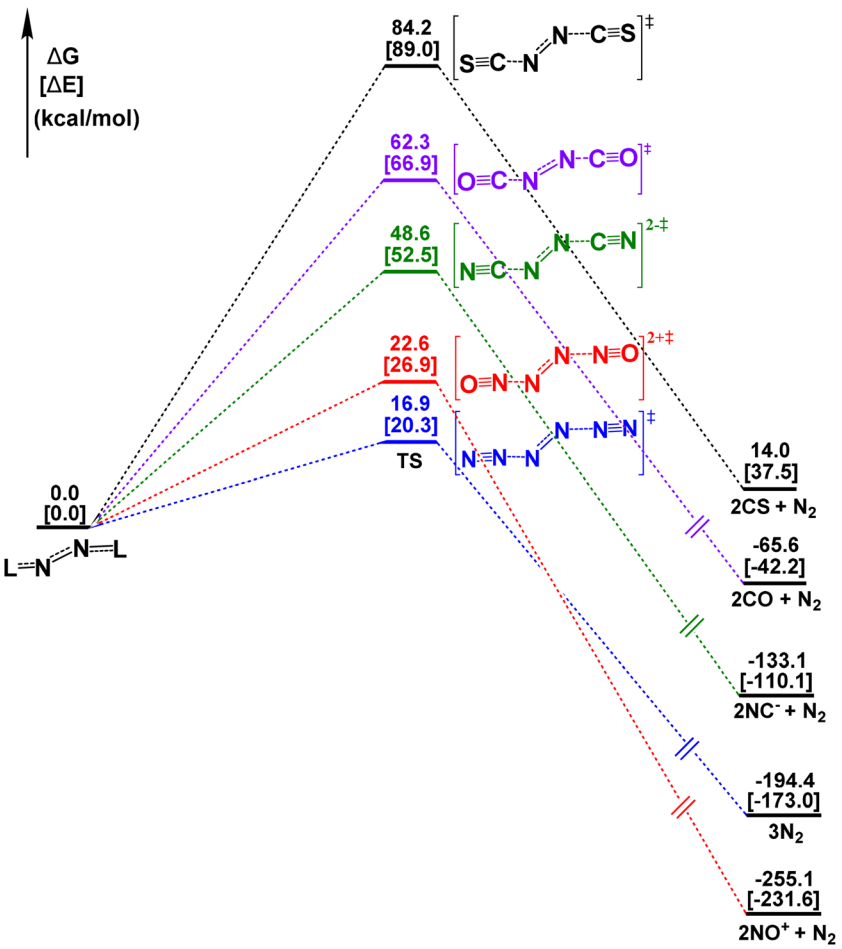

Fig. 2 Energy profile for the reaction $N_2L_2 \rightarrow N_2 + 2L$ at the CCSD(T)/cc-pVTZ//M06-2X/cc-pVTZ level.

accounts for the experimental finding that N_6 directly dissociated into 3 N_2. The same applies for $N_2(CO)_2$, which photolytically dissociates into N_2 + 2 CO whereas cleavage into NCO radical was observed only to a small extent.[22a]

Examination of the transition state structures for the dissociation reaction reveals surprising features (Fig. 3). The geometries of $[N_2L_2]^{\neq}$ possess a non-planar staggered geometry with a *syn* conformation of the ligands except for $[N_2(CS)_2]^{\neq}$, which exhibits a nearly linear NNCS moiety with one CS ligand, where the bond to the second CS ligand is significantly stretched. This implies that the fragmentation reaction may possibly be a two-step process in which an intermediate product, NN-L is formed along the dissociation reaction. We calculated the intrinsic reaction coordinate starting from the transition states and found that it smoothly connects to the reaction products N_2 + 2L. The fragmentation reaction is thus predicted as a concerted but highly asynchronous process where the two N_2–L bonds break one after the other. Note that the central N–N bond of the transition state $[N_2L_2]^{\neq}$ is clearly shorter than in the equilibrium structures.

Hexanitrogen was clearly identified by spectroscopic signals, and the authors presented a careful analysis of the vibrational spectrum of the molecule.[6] The IR spectrum of N_6 exhibits an intense vibrational band at 2076.6 cm^{-1}, which comes from an asymmetric stretching mode of the terminal N_2 ligands. Fig. 4 shows the calculated IR spectra of the five molecules N_2L_2. They show a similar pattern where the asymmetric stretching mode ν_{as} of the terminal L_2 ligands, which has the second largest wavenumber of all 12 fundamentals, exhibits the strongest signal. The symmetric stretching mode ν_s with a slightly higher wavenumber is IR inactive. The calculated wavenumber of 2263.7 cm^{-1} for the asymmetric mode of N_6 is blue shifted for L = CO (Δ = 55 cm^{-1}) and L = NO^+ (Δ = 118 cm^{-1}), but it is red shifted for L = CS (Δ = −242 cm^{-1}) and L = CN^- (Δ = −133 cm^{-1}). The calculated frequency shift of the intense asymmetric stretching mode ν_s is very helpful information for identifying the molecules.

In addition to N_6 $[N_2(N_2)_2]$, the complexes $N_2(CO)_2$ and $N_2(CS)_2$ have been synthesised and identified spectroscopically and they were also the subject of theoretical works. The

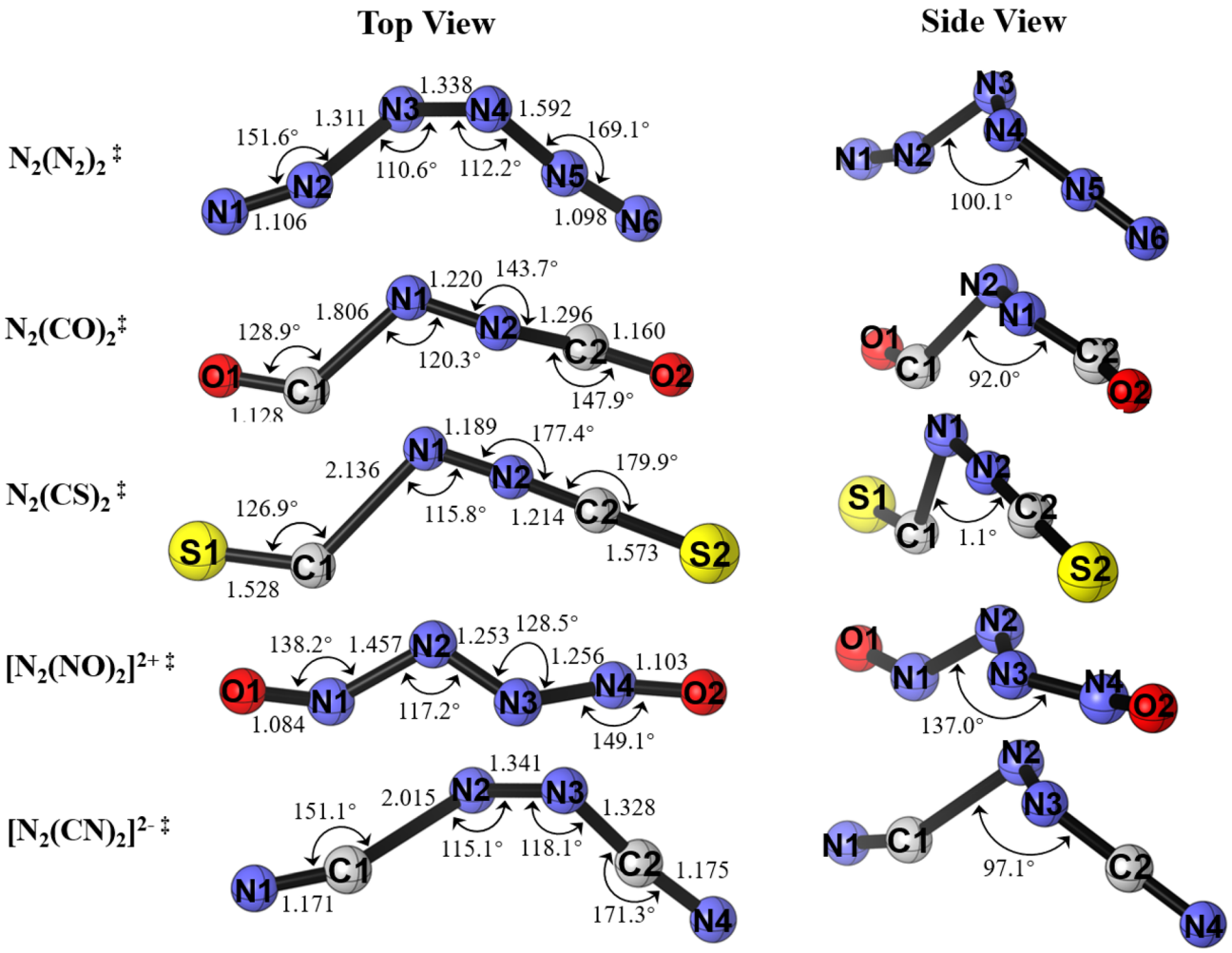

Fig. 3 Geometries of the transition states of N_2L_2 (L = N_2, CO, CS, CN^-, NO^+) compounds for the dissociation into 2L and N_2 at the M06-2X/cc-pVTZ level. The top view gives the bond lengths and bond angles, and the side view gives the dihedral angles L-N_2-L. The bond lengths are given in Å and the angles in degree.

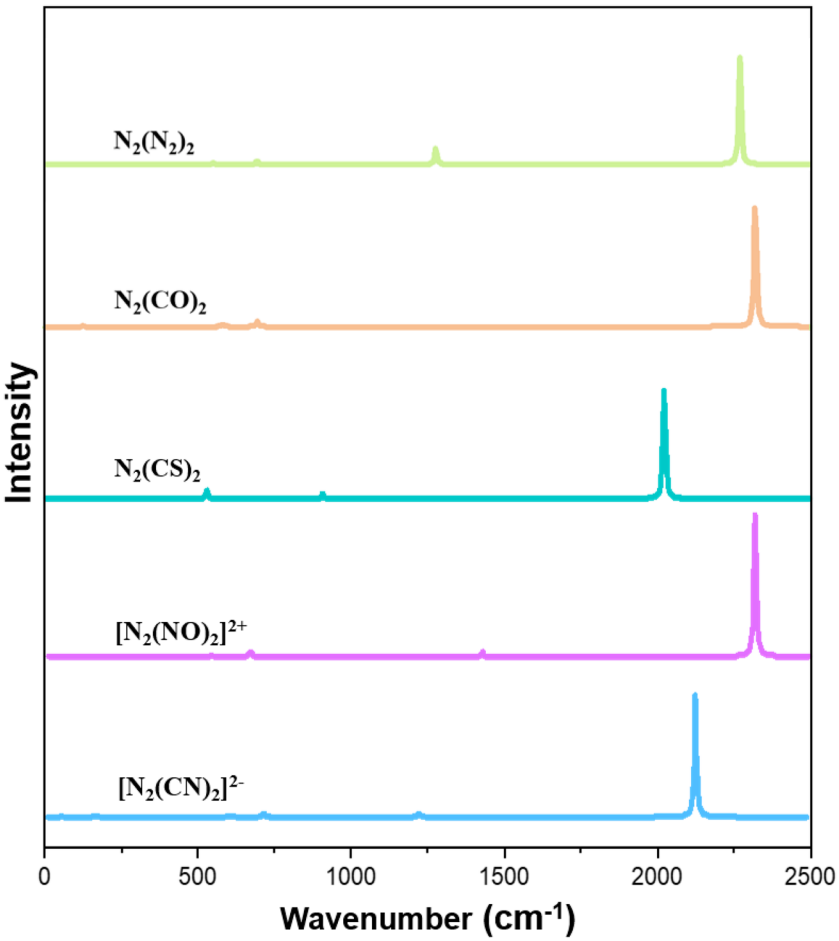

Fig. 4 Calculated IR spectra of N_2L_2 complexes (L = N_2, CO, CS, CN^-, NO^+) at the M06-2X/cc-pVTZ level.

dicarbonyl adduct was introduced as diisocynate O═C═N–N═C═O following the conventional descriptions using Lewis structures.[22] Photolysis of the matrix-isolated $N_2(CO)_2$ gives N_2 + 2 CO as products, which agrees with our calculated reaction profile (Fig. 2). The IR spectrum shows one very intensive band at 2200.6 cm^{-1} for the asymmetric NCO stretching mode besides several signals with lower intensity.[22a] The comparison with the IR spectrum of N_6 gives a red shift of 124 cm^{-1}, which agrees with the direction but is higher than our computed value of 54 cm^{-1}. The diisothiocyanate complex $N_2(CS)_2$ was identified as product of the photolysis of the energetically lower lying isomer $S_2(CN)_2$ with a characteristic vibrational mode of the IR spectrum at 1910 cm^{-1}.[23] The experimental red-shift compared to the asymmetric stretching mode of N_6 is also given by our calculations, but the observed value of −166 cm^{-1} is smaller than our computed value of −242 cm^{-1}. The computed wavenumber for $[N_2(NO)_2]^{2+}$ (2382 cm^{-1}) agrees quite well with the experimental value of NO^+ (2340 cm^{-1}) whereas the calculated value for $[N_2(CN)_2]^{2-}$ (2131 cm^{-1}) is red-shifted compared with an approximately interaction-free anion CN^- (2244 cm^{-1}).[24] The complete set of the calculated vibrational spectra of the five molecules N_2L_2 is given in Table S4 of the SI.

We analyzed the bonding situation in N_2L_2 with a variety of methods. Fig. 1 shows that the Mayer bond order (MBO) of the central N–N bond is between 0.83 (L = CN^-) and 0.96 (L = CS), which is a rather small variation considering the differences in the N–N bond length between 1.488 Å (L = CN^-) and 1.355 Å (L = CS). The atomic partial charges suggest that there is a total charge donation in the neutral complexes L→(N_2)←L with 0.98 *e* (L = CO), 0.78 *e* (L = CS), and 0.56 *e* (L = N_2). There is an even stronger charge donation of 1.38 *e* in the dianion (L = CN^-) and a small backdonation in reverse direction L←(N_2)→L with 0.10 *e* in the dication (L = NO^+).

We proposed in our earlier study that the diatomic N_2 species in $N_2(PPh_3)_2$ binds through its highly excited $(1)^1\Gamma_g$ state where the out-of-plane π and π* orbitals are doubly occupied.[4] Fig. 5 shows schematically the valence MOs of N_2 in the $(1)^1\Gamma_g$ state. The donation of the L_2 ligands L→(N_2)←L may take place into the vacant $1\pi_u'$ (bonding) and $1\pi_g'$ (antibonding) orbitals of N_2. Note that the assignment of π symmetry refers to free N_2, which has two mirror planes that contain the atoms. The complexes L-N_2-L have only one mirror plane and the donation is correctly assigned as in-plane σ(+,−) and σ(+,+) orbital interaction.

There are two occupied out-of-plane π MOs, $1\pi_u$ (bonding) and $1\pi_g$ (antibonding), in the $(1)^1\Gamma_g$ state of N_2. If this holds true also for the N_2L_2 complexes in the present study, the number of occupied valence π MOs should be four (π and π*

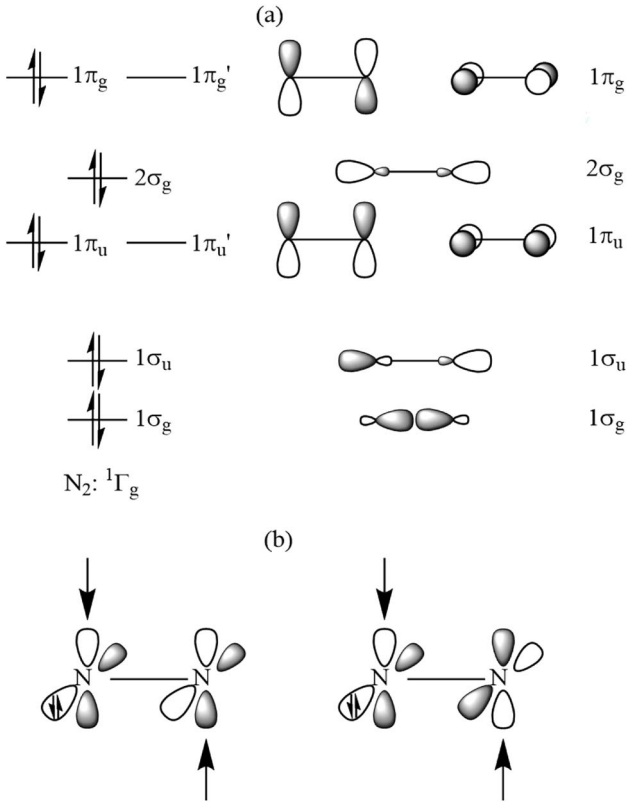

Fig. 5 (a) Schematic representation of the $(1)^1\Gamma_g$ state of N_2 and the associated orbitals. (b) Donation of the plus and minus combination of the lone-pair donor orbitals of L into the vacant in-plane π and π* orbitals of N_2. The orbital numbering refers to the valence orbitals of N_2.

from N_2 and one π from each ligand L) and not three. Examination of the shape of the Kohn–Sham MOs shows that this is indeed the case. Fig. 6 displays the four occupied valence π MOs of N_6. The number of nodes follows the common symmetry rules with zero (HOMO-8), one (HOMO-7), two (HOMO-2), and three (HOMO). The same number of occupied valence π is found for the other N_2L_2 complexes. The complete set of occupied valence MOs of all N_2L_2 complexes is presented in Fig. S2–S6. Fig. 6 shows also the HOMO of the N_2L_2 complexes, which can be identified with the out-of-plane π* orbital of N_2 mixing with the antibonding π* orbitals of the ligands L.

A more detailed insight into the nature of the N_2–L_2 bonds is provided by the EDA-NOCV analysis of the interactions between the fragments. In our previous study of $N_2(PPh_3)_2$, we considered only neutral N_2 in the excited $(1)^1\Gamma_g$ state and 2 PPh_3 ligands in the electronic ground state.[4] We analyzed N_2L_2 using various electronic states and charges of the fragments N_2 and 2L. Numerous studies have shown that the strength of the orbital term ΔE_{orb}, which considers the change in the wave function during bond formation, is a reliable indicator of the optimal fragments for describing the bond between them.[7,25] The fragments with the lowest absolute values of ΔE_{orb} are the best choice for explaining the bonding interactions. Table 2 shows the numerical results for L = N_2.

It becomes obvious that the chemical bonds in N_6 between the central N_2 moiety and the terminal N_2 species are indeed best described in terms of dative interactions $N_2 \rightarrow (N_2) \leftarrow N_2$ between central N_2 in the excited $(1)^1\Gamma_g$ singlet state and two terminal N_2 fragments in the $^1\Sigma_g^+$ electronic ground state. The interactions between central N_2 in the $^3\Sigma_u^+$ triplet state and the terminal ligands in the symmetry-adapted $(N_2)_2$ triplet state, which exhibit a mixture of electron-sharing and dative bonds, give a bigger ΔE_{orb} value. The same holds for the formation of electron-sharing double bonds between central N_2 in the $^5\Sigma_u^+$ quintet state and the terminal ligands in the symmetry-adapted $(N_2)_2$ quintet state. EDA-NOCV calculations using central N_2^- as an anion in the electronic doublet ($^2\Sigma_g^+$) or quartet ($^4\Sigma_u^+$) state and the terminal $(N_2)_2^+$ ligand as a cation in the symmetry-adapted doublet or quartet state also result in bigger ΔE_{orb} values.

Further examination of the dative interactions between central N_2 and the terminal N_2 ligands reveals that they come mainly from $N_2 \rightarrow (N_2)$ N_2 σ donation through out-of-phase ($\Delta E_{orb(1)}$) and in-phase ($\Delta E_{orb(2)}$) orbital pairs, which provide 75% of the total orbital (covalent) bonding. The π backdonation $N_2 \leftarrow (N_2) \rightarrow N_2$ *via* out-of-phase ($\Delta E_{orb(3)}$) and in-phase ($\Delta E_{orb(4)}$) orbital interactions deliver only 17% of ΔE_{orb}. The nature of the individual orbital interactions $\Delta E_{orb(1)}$–$\Delta E_{orb(4)}$ becomes clear when considering the corresponding deformation densities and the associated orbitals, which are shown in Fig. 7. The dominant orbital interactions through (+,−) and (+,+) σ donation $N_2 \rightarrow (N_2) \leftarrow N_2$ nicely explain the bond shortening of the central N_2 moiety compared to free N_2 in the $^1\Gamma$ state, which has

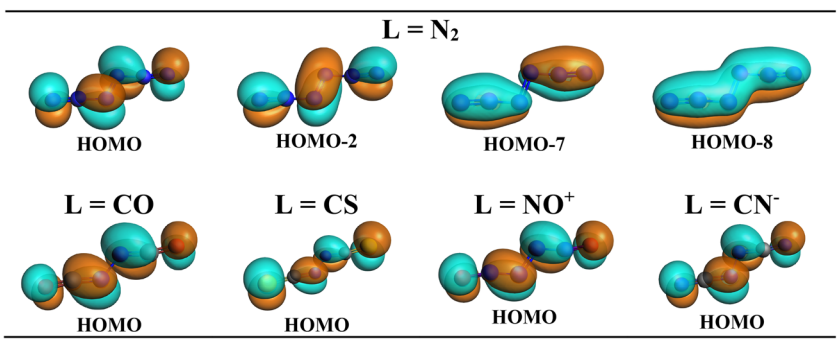

Fig. 6 Top row: plot of the four occupied valence π MOs of N_6. Bottom row: plot of the HOMO of N_2L_2 with L = CO, CS, NO^+, CN^-.

Table 2 EDA-NOCV results of the complex N_2L_2 (L = N_2) considering L_2 as one fragment and central N_2 as another fragment at the M06-2X/TZ2P-ZORA//CCSD(T)/cc-pVTZ level. Energy values are given in kcal mol^{-1}

Energies	Orbital interaction	N_2 (singlet) + 2L (singlet)	N_2 (triplet) + 2L (triplet)	N_2 (quintet) + 2L (quintet)	N_2^-(doublet) + 2L$^+$ (doublet)	N_2^-(quartet) + 2L$^+$ (quartet)
ΔE_{int}		−165.0	−368.7	−401.3	−387.3	−519.0
ΔE_{Pauli}		1036.0	1022.8	1028.3	1042.8	1090.1
ΔE_{elstat}[a]		−364.9 (30.4%)	−388.8 (27.9%)	−438.1 (30.6%)	−538.1 (37.6%)	−615.1 (38.6%)
ΔE_{orb}[a]		−836.1 (69.6%)	−1002.7 (72.1%)	−991.5 (69.4%)	−894.5 (62.4%)	−980.0 (61.4%)
$\Delta E_{orb(1)}$[b]	L–NN–L σ-bond (+,−)	−328.7 (39.3%)	−317.3 (31.6%)	−328.7 (33.2%)	−329.8 (36.9%)	−350.4 (35.8%)
$\Delta E_{orb(2)}$[b]	L–NN–L σ-bond (+,+)	−296.4 (35.5%)	−296.9 (29.6%)	−314.1 (31.7%)	−261.4 (29.2%)	−337.7 (34.5%)
$\Delta E_{orb(3)}$[b]	L–NN–L π-bond (+,−)	−98.6 (11.8%)	−174.9 (17.4%)	−151.4 (15.3%)	−123.1 (13.8%)	−90.9 (9.3%)
$\Delta E_{orb(4)}$[b]	L–NN–L π-bond (+,+)	−44.7 (5.3%)	−86.5 (8.6%)	−94.8 (9.6%)	−54.0 (6.0%)	−56.2 (5.7%)
$\Delta E_{orb(rest)}$[b]		−67.7 (8.1%)	−127.1 (12.7%)	−102.2 (10.3%)	−126.2 (14.1%)	−144.8 (14.8%)

[a] The values in parentheses give the percentage contribution to the total attractive interactions $\Delta E_{elstat} + \Delta E_{orb}$. [b] The values in parentheses give the percentage contribution to the total orbital interactions ΔE_{orb}.

a calculated bond length of 1.608 Å and is 294.3 kcal mol^{-1} above the $X^1\Sigma_g^+$ ground state.[8] The donation takes place into the vacant in-plane and out-of-plane π orbitals of N_2, which are bonding orbitals (see Fig. 5). Note that the $(1)^1\Gamma_g$ state of N_2 is a reference state which is strongly stabilized by the orbital interaction. It is not formed as a free species during the reaction process.

The numerical EDA-NOCV results of the other N_2L_2 compounds are given in Tables S5–S8 of SI. In contrast to the results for N_6, the lowest ΔE_{orb} values with L = CO, CS, NO^+ are calculated for the interactions between the central N_2 in the $^5\Sigma_u^+$ quintet state and the terminal ligands in the symmetry-adapted $(L)_2$ quintet state, which indicate electron-sharing double bonds between the fragments. The central N–N bond in the latter species is much shorter (between 1.355–1.386 Å) than in N_6 (1.450 Å). The lowest ΔE_{orb} value of N_2L_2 with L = CN^- is found for the interactions between N_2^- in the electronic quartet ($^4\Sigma_u^+$) state and the terminal $(CN)_2^-$ ligands as symmetry-adapted quartets. The individual orbital interactions are identified by the corresponding deformation densities and the associated orbitals, which are shown in Fig. S7–S14. The latter electron-sharing interactions also lead to four occupied π valence MOs in all five N_2L_2 molecules.

In order to compare the N_2L_2 compounds with each other, we have chosen the same fragments with the central N_2 in the excited $(1)^1\Gamma_g$ singlet state and two terminal N_2 fragments in the

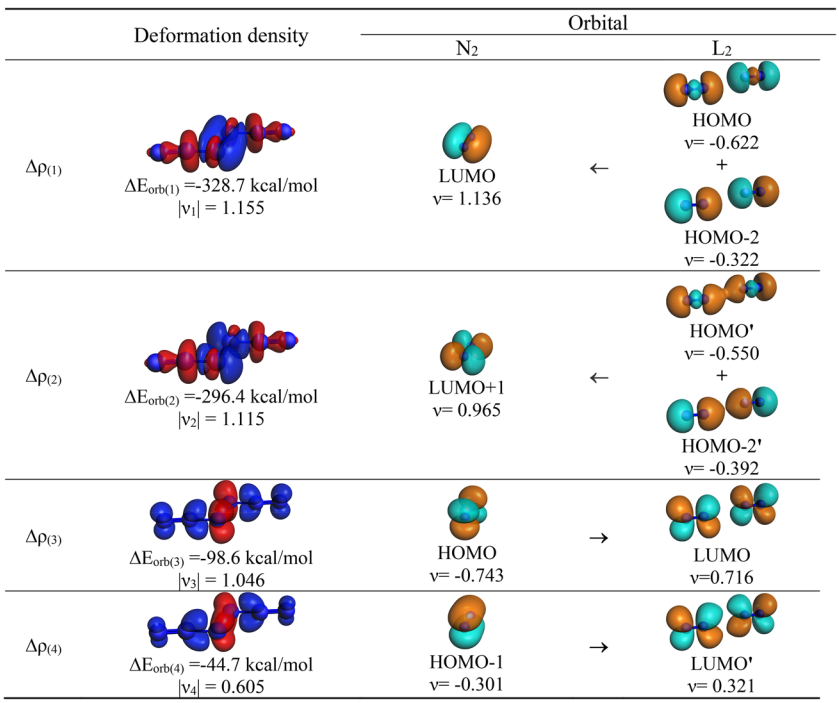

Fig. 7 Plot of the deformation densities, $\Delta\rho_{(1-4)}$ shown as the electronic charge corresponding to $\Delta E_{orb(1-4)}$ and the related interacting orbitals of N_2L_2 (L = N_2) at the M06-2X/TZ2P-ZORA//CCSD(T)/cc-pVTZ level using NN ($^1\Gamma_g$) + L_2 (singlet) as interacting fragments. The eigenvalues ν indicate the size of the charge flow. The direction of charge flow is red → blue. The isovalue for $\Delta\rho_{(1-4)}$ is 0.003 au.

Table 3 EDA-NOCV results of complexes N_2-L_2 (L = N_2, CO, CS, NO^+, CN^-) considering L_2 as one fragment and central N_2 as another fragment in the singlet states ($^1\Gamma_g$ state of N_2 and symmetry adapted singlet state of L_2) at the M06-2X/TZ2P-ZORA//CCSD(T)/cc-pVTZ level. Energy values are given in kcal mol^{-1}

Energies	Orbital interaction	L = N_2	L = CO	L = CS	L = NO^+	L = CN^-
ΔE_{int}		−165.0	−306.0	−387.0	−202.5	−301.4
ΔE_{Pauli}		1036.0	1400.4	1542.2	1242.3	1155.6
ΔE_{elstat} [a]		−364.9 (30.4%)	−530.8 (31.1%)	−595.4 (30.9%)	−356.9 (24.7%)	−484.9 (33.3%)
ΔE_{orb} [a]		−836.1 (69.6%)	−1175.7 (68.9%)	−1333.8 (69.1%)	−1088.0 (75.3%)	−972.1 (66.7%)
$\Delta E_{orb(1)}$ [b]	L–NN–L in-plane(σ)-bond (+,−)	−328.7 (39.3%)	−483.0 (41.1%)	−536.4 (40.2%)	−373.2 (34.3%)	−405.8 (41.7%)
$\Delta E_{orb(2)}$ [b]	L–NN–L in-plane(σ)-bond (+,+)	−296.4 (35.5%)	−434.3 (37.4%)	−493.4 (37.0%)	−322.3 (29.6%)	−400.0 (41.1%)
$\Delta E_{orb(3)}$ [b]	L–NN–L out-of-plane(π)-bond (+,−)	−98.6 (11.8%)	−76.1 (6.5%)	−134.6 (10.1%)	−182.1 (16.7%)	−70.4 (7.2%)
$\Delta E_{orb(4)}$ [b]	L–NN–L out-of-plane(π)-bond (+,+)	−44.7 (5.3%)	−45.2 (3.8%)	−48.0 (3.6%)	−75.5 (6.9%)	−34.6 (3.6%)
$\Delta E_{orb(rest)}$ [b]		−67.7 (8.1%)	−137.1 (11.7%)	−121.4 (9.1%)	−134.9 (12.4%)	−61.3 (6.3%)

[a] The values in parentheses give the percentage contribution to the total attractive interactions $\Delta E_{elstat} + \Delta E_{orb}$. [b] The values in parentheses give the percentage contribution to the total orbital interactions ΔE_{orb}.

$^1\Sigma_g^+$ electronic ground state as model for the bonding interactions. Table 3 gives the numerical results. The calculated interaction energies ΔE_{int} show the same order CS > CO > CN^- > NO^+ > N_2 as the calculated activation barriers $\Delta E^{\neq}$ (Fig. 2), which indicates that the choice of the singlet fragments is a valid model for the trend of the chemical bonds. The orbital (covalent) interactions always make the largest percentage contribution to the chemical bonds, which is particularly high for L = NO^+ (75%). The breakdown of ΔE_{orb} into the pairwise orbital interactions reveals that the σ donations through out-of-phase ($\Delta E_{orb(1)}$) and in-phase ($\Delta E_{orb(2)}$) orbital pairs are always the largest components of the total orbital bonding. The percentage contribution of $\Delta E_{orb(1)}$ and $\Delta E_{orb(2)}$ is higher for L = CN^- and lower for L = NO^+, which is due to the charges of the ligands. A surprising result concerns the low contribution of the π backdonation $\Delta E_{orb(3)}$ and $\Delta E_{orb(4)}$ for L = CO, which is smaller than for L = N_2. CO is known to be a better π acceptor than N_2 in transition metal complexes.[26] The peculiar results for the orbital interactions in the neutral N_2L_2 compounds can be explained with the dominance of the σ donation L→N_2←L over π backdonation L←N_2→L, which comes to the fore by the calculated partial charges (Fig. 1). The energy of the σ lone-pair HOMO suggests that the donor strength of the ligands has the order CS (ε = −10.1 eV) > CO (ε = −12.2 eV) > N_2 (ε = −13.9 eV). But the overall strength of the dative interactions cannot simply be derived from the orbital interactions. The orbital interaction ΔE_{orb} of the negatively charged CN^- is significantly weaker (−972.1 kcal mol^{-1}) than that of NO^+ (−1088.0 kcal mol^{-1}), but the total interaction energy ΔE_{int} of the former ligand is clearly higher (−301.4 kcal mol^{-1}) than the latter (−202.5 kcal mol^{-1}). The electrostatic interaction ΔE_{elstat} but also the Pauli repulsion ΔE_{Pauli}, which makes the largest contribution to ΔE_{int}, are equally relevant for the trend of the interatomic interactions. It has been shown that the Pauli repulsion is the crucial factor for the equilibrium geometry of molecules.[27]

We also want to comment on the $\Delta E_{orb(rest)}$ term, which is comparatively large in the systems with L = CO, CS, NO^+. It stems from the relaxation of the fragment orbitals with respect to the isolated species. The central N_2 moieties in the latter complexes have significantly shorter N–N distances than in the $^1\Gamma_g$ singlet state (1.606 Å at the M06-2X/cc-pVTZ level), and the electronic relaxation is, therefore, larger than in the complexes with L = N_2, CN^- which have longer central N–N bonds (Fig. 1). The impact of the geometry relaxation on the BDE and the stability of molecules has been pointed out by Bickelhaupt in his activation strain model.[28] The strong influence of the fragment relaxation and the geometry of the interacting species becomes obvious when the trend of the interaction energy ΔE_{int} between the frozen fragments (L = CS > CO > CN^- > NO^+ > N_2) is compared with the BDEs that are calculated using the fragments at their equilibrium geometries and electronic ground state (L = CS > CO > CN^- > N_2 > NO^+). Finally, we want to mention that the chemistry of $N_2(PPh_3)_2$ was recently studied in joint experimental and theoretical works by the groups of Stephan and Grimme, which showed a surprising reactivity of the member of the N_2L_2 compound class.[29]

Summary and conclusion

Geometry optimizations of the compounds N_2L_2 (L = N_2, CO, CS, NO^+, CN^-) at the CCSD(T)/cc-pVTZ level give the energy minimum structures with a *trans*-periplanar arrangement of the L_2 ligands at the N_2 unit. Attempts to localize a *syn* isomer failed, and the calculations gave the *trans* isomer as the only conformational minimum. Energy calculations suggest that all compounds N_2L_2 (L = N_2, CO, CS, NO^+, CN^-) may be synthesized and should be observable under appropriate conditions. The complexes with L = N_2, CO, NO^+, CN^- are predicted as thermodynamically unstable for dissociation into N_2 + 2 L with ΔG^{298} value lying in between −257 kcal mol^{-1} (L = NO^+) and −73 kcal mol^{-1} (L = CO), but the adduct $N_2(CS)_2$ is calculated as slightly stable with ΔG^{298} = 4 kcal mol^{-1}. The homolytic dissociation reaction into two fragments N_2L_2 → 2 NL is energetically less favorable than the heterolytic fragmentation N_2L_2 → N_2 + 2 L, which proceeds synchronously but asymmetrically. The activation barriers for the fragmentation reaction N_2L_2 → N_2 + 2 L have values between $\Delta G^{\neq}$(298 K) = 17 kcal mol^{-1} for L = N_2 and $\Delta G^{\neq}$(298 K) = 84 kcal mol^{-1} for L = CS. The calculated vibrational frequencies show that all molecules N_2L_2 have a characteristic vibrational mode with the

second highest wavenumber ν_{as} that comes from the antisymmetric stretch of the ligands L, which is blue shifted for L = CO ($\Delta = 55$ cm^{-1}) and L = NO$^+$ ($\Delta = 118$ cm^{-1}) but it is red shifted for L = CS ($\Delta = -54$ cm^{-1}) and L = CN$^-$ ($\Delta = -133$ cm^{-1}) relative to the ν_{as} mode of L = N_2.

The analysis of the bonding situation using the charge distribution reveals that there is a total charge donation L→(N$_2$)←L in all complexes ranging between 1.38 *e* (L = CN$^-$) and 0.56 *e* (L = N_2), except in the dication with L = NO$^+$, where a small backdonation in reverse direction L→(N$_2$)←L with 0.10 *e* is calculated. EDA-NOCV calculations of N_6 using the central N_2 moiety and the terminal N_2 ligands as interacting fragments in various electronic states and with different partial charges show that the best description of the bonding situation is given in terms of dative interactions N_2→(N_2)←N_2 between central N_2 in the excited (1)$^1\Gamma_g$ singlet state and the terminal N_2 fragments in the $^1\Sigma_g^+$ electronic ground state. In contrast to the results for N_6, the best description of the complexes with L = CO, CS, NO$^+$ is calculated for the interactions between the central N_2 in the $^5\Sigma_u^+$ quintet state and the terminal ligands in the symmetry-adapted $(L)_2$ quintet state, which indicates electron-sharing double bonds between the fragments. For N_2L_2 with L = CN$^-$, it is found that the bonding is best described for the interaction between N_2^- in the electronic quartet ($^4\Sigma_u^+$) state and the terminal $(L)_2^-$ ligand as symmetry-adapted quartet. A comparative analysis of the five N_2L_2 compounds using the same fragments with central N_2 in the excited (1)$^1\Gamma_g$ singlet state and the terminal L_2 fragments in the $^1\Sigma_g^+$ electronic ground state reveals that the σ donation L→(N$_2$)←L makes the largest contribution to the stabilizing interactions and that the π backdonation L←(N$_2$)←L is much weaker. In contrast to the common bonding model for N_6 using Lewis structures N$^-$=N$^+$=N–N=N$^+$=N$^-$, the donor–acceptor model N_2→(N_2)←N_2 explains that the lowest activation barrier is found for the concerted cleavage of the two formal double bonds, leading to the experimentally observed dissociation into 3 N_2.

Author contributions

G. F. and S. P. conceived the project, wrote the draft and finalized it, Y. L., C. D. and L. X. performed the calculations, Y. L. analyzed the data. All authors took part in the discussions and approved the final version.

Conflicts of interest

The authors declare no conflict of interest.

Data availability

The data supporting this article have been included as part of the supplementary information (SI). Supplementary information is available. See DOI: https://doi.org/10.1039/d5sc08399k.

Acknowledgements

GF acknowledges financial support by Nanjing Tech University. SP is grateful for financial assistance by Jilin University.

References

1 R. Appel and R. Schöllhorn, *Angew. Chem., Int. Ed.*, 1964, **3**, 805.
2 R. Appel, B. Blaser and G. Siegemund, *Z. Anorg. Allg. Chem.*, 1968, **363**, 176–182.
3 D. J. Wilson, S. A. Couchman and J. L. Dutton, *Inorg. Chem.*, 2012, **51**, 7657–7668.
4 N. Holzmann, D. Dange, C. Jones and G. Frenking, *Angew. Chem., Int. Ed.*, 2013, **52**, 3004–3008.
5 M. Reinmuth, C. Neuhäuser, P. Walter, M. Enders, E. Kaifer and H.-J. Himmel, *Eur. J. Inorg. Chem.*, 2011, **2011**, 83–90.
6 W. Qian, A. Mardyukov and P. R. Schreiner, *Nature*, 2025, **642**, 356–360.
7 C&EN, *Am. Chem. Soc.*, 2025, vol. 103, 23.
8 M. Hochlaf, H. Ndome, D. Hammoutène and M. Vervloet, *J. Phys. B: At. Mol. Opt. Phys.*, 2010, **43**, 245101.
9 Q. Wang, S. Pan, S. Lei, J. Jin, G. Deng, G. Wang, L. Zhao, M. Zhou and G. Frenking, *Nat. Commun.*, 2019, **10**, 3375.
10 (*a*) Y. Zhao and D. G. Truhlar, *Theor. Chem. Acc.*, 2008, **120**, 215–241; (*b*) T. H. Dunning, Jr, *J. Chem. Phys.*, 1989, **90**, 1007–1023.
11 G. D. Purvis III and R. J. Bartlett, *J. Chem. Phys.*, 1982, **76**, 1910–1918.
12 M. J. Frisch, G. W. Trucks, H. B. Schlegel, G. E. Scuseria, M. A. Robb, J. R. Cheeseman, G. Scalmani, V. Barone, G. A. Petersson, H. Nakatsuji, X. Li, M. Caricato, A. V. Marenich, J. Bloino, B. G. Janesko, R. Gomperts, B. Mennucci, H. P. Hratchian, J. V. Ortiz, A. F. Izmaylov, J. L. Sonnenberg, D. Williams-Young, F. Ding, F. Lipparini, F. Egidi, J. Goings, B. Peng, A. Petrone, T. Henderson, D. Ranasinghe, V. G. Zakrzewski, J. Gao, N. Rega, G. Zheng, W. Liang, M. Hada, M. Ehara, K. Toyota, R. Fukuda, J. Hasegawa, M. Ishida, T. Nakajima, Y. Honda, O. Kitao, H. Nakai, T. Vreven, K. Throssell, J. A. Montgomery Jr, J. E. Peralta, F. Ogliaro, M. J. Bearpark, J. J. Heyd, E. N. Brothers, K. N. Kudin, V. N. Staroverov, T. A. Keith, R. Kobayashi, J. Normand, K. Raghavachari, A. P. Rendell, J. C. Burant, S. S. Iyengar, J. Tomasi, M. Cossi, J. M. Millam, M. Klene, C. Adamo, R. Cammi, J. W. Ochterski, R. L. Martin, K. Morokuma, O. Farkas, J. B. Foresman and D. J. Fox, *Gaussian 16 Rev. B.01*, Wallingford, CT, 2016.
13 I. Mayer, *Chem. Phys. Lett.*, 1983, **97**, 270–274.
14 E. D. Glendening, C. R. Landis and F. Weinhold, *J. Comput. Chem.*, 2019, **40**, 2234–2241.
15 T. Lu and F. Chen, *J. Comput. Chem.*, 2012, **33**, 580–592.
16 T. Ziegler and A. Rauk, *Theor. Chim. Acta*, 1977, **46**, 1–10.
17 (*a*) M. Mitoraj and A. Michalak, *Organometallics*, 2007, **26**, 6576–6580; (*b*) M. Mitoraj and A. Michalak, *J. Mol. Model.*, 2008, **14**, 681–687.

18 (*a*) E. Van Lenthe and E. J. Baerends, *J. Comput. Chem.*, 2003, **24**, 1142–1156; (*b*) E. van Lenthe, J. G. Snijders and E. J. Baerends, *J. Chem. Phys.*, 1996, **105**, 6505–6516.

19 (*a*) G. te Velde, F. M. Bickelhaupt, E. J. Baerends, C. Fonseca Guerra, S. J. A. van Gisbergen, J. G. Snijders and T. Ziegler, *J. Comput. Chem.*, 2001, **22**, 931–967; (*b*) *ADF 2020, ADF SCM, Theoretical Chemistry, Vrije Universiteit*, Amsterdam, The Netherlands, https://www.scm.com/.

20 (*a*) A. Michalak, M. Mitoraj and T. Ziegler, *J. Phys. Chem. A*, 2008, **112**, 1933–1939; (*b*) M. P. Mitoraj, A. Michalak and T. Ziegler, *J. Chem. Theory Comput.*, 2009, **5**, 962–975.

21 (*a*) L. Zhao, S. Pan and G. Frenking, *Energy Decomposition Analysis of the Chemical Bond: Scope and Limitation in Comprehensive Computational Chemistry*, ed. M. Yáñez and R. J. Boyd, Elsevier, Oxford, 2024, vol. 2, pp. 322–361; (*b*) F. M. Bickelhaupt, C. Fonseca Guerra, M. Mitoraj, F. Sagan, A. Michalak, S. Pan and G. Frenking, *Phys. Chem. Chem. Phys.*, 2022, **24**, 15726–15735; (*c*) L. Zhao, M. Hermann, W. H. E. Schwarz and G. Frenking, *Nat. Rev. Chem.*, 2019, **3**, 48–63; (*d*) L. Zhao, S. Pan, N. Holzmann, P. Schwerdtfeger and G. Frenking, *Chem. Rev.*, 2019, **119**, 8781–8845.

22 (*a*) G. Maier, M. Naumann, H. P. Reisenauer and J. Eckwert, *Angew Chem. Int. Ed. Engl.*, 1996, **35**, 1696–1697; (*b*) T. Pasinszki, *Phys. Chem. Chem. Phys.*, 2008, **10**, 1411–1418.

23 T. Vörös, G. Bazsó, G. Tarzay and T. Pasinszki, *J. Mol. Struct.*, 2012, **1025**, 117–123.

24 T. A. Engesser, C. Friedmann, A. Martens, D. Kratzert, P. J. Malinowski and I. Krossing, *Chem. Eur. J.*, 2016, **22**, 15085–15094.

25 (*a*) D. M. Andrada, J. L. Casals-Sainz, Á. Martín Pendás and G. Frenking, *Chem. Eur. J.*, 2018, **24**, 9083–9089; (*b*) P. Jerabek, P. Schwerdtfeger and G. Frenking, *J. Comput. Chem.*, 2019, **40**, 247–264; (*c*) R. Saha, S. Pan, G. Merino and P. K. Chattaraj, *Angew. Chem., Int. Ed.*, 2019, **58**, 8372–8377; (*d*) W. Su, Y. Ma, L. Xiang, J. Wang, S. Wang, L. Zhao, G. Frenking and Q. Ye, *Chem. Eur. J.*, 2021, **27**, 10006–10011; (*e*) C. Ding, L. Yao, L. Zhao and G. Frenking, *Phys. Chem. Chem. Phys.*, 2022, **24**, 16732–16745; (*f*) R. Liu, L. Qin, Z. Zhang, L. Zhao, F. Sagan, M. Mitoraj and G. Frenking, *Chem. Sci.*, 2023, **14**, 4872–4887; (*g*) L. Qin, R. Liu, F. Sagan, Z. Zhang, L. Zhao, M. Mitoraj and G. Frenking, *Phys. Chem. Chem. Phys.*, 2024, **26**, 24294–24313; (*h*) L. Qin, Y.-q. Liu, R. Liu, X. Yang, Z.-h. Cui, L. Zhao, S. Pan, S. Fau and G. Frenking, *Chem. Eur. J.*, 2024, **30**, e202304136; (*i*) W.-X. Chen, W.-J. Tian, Z.-S. Li, J.-J. Wang, A. Muñoz-Castro, G. Frenking and Z.-M. Sun, *Nat. Synth.*, 2025, **4**, 471–478; (*j*) Y.-H. Xu, X. Yang, Y.-N. Yang, L. Zhao, G. Frenking and Z.-M. Sun, *Nat. Chem.*, 2025, **17**, 556–563.

26 G. Frenking and N. Fröhlich, *Chem. Rev.*, 2000, **100**, 717–774.

27 A. Krapp, F. M. Bickelhaupt and G. Frenking, *Chem. Eur. J.*, 2006, **12**, 9196–9216.

28 I. Fernandez and F. M. Bickelhaupt, *Chem. Soc. Rev.*, 2014, **43**, 4953–4967.

29 (*a*) L. Miao, J. Yeung, A. Yeganeh-Salman, Z.-w. Qu, S. Grimme and D. W. Stephan, *J. Am. Chem. Soc.*, 2025, **147**, 4720–4725; (*b*) V. Bedi, A. N. L. Ocampochua, Z.-W. Qu, S. Grimme and D. W. Stephan, *Angew. Chem., Int. Ed.*, 2025, **64**, e202503331.